5

METAL–POLYMER NANOCOMPOSITE SYNTHESIS: NOVEL *EX SITU* AND *IN SITU* APPROACHES

G. Carotenuto and L. Nicolais

Institute of Composite and Biomedical Materials, National Research Council, Naples, Italy

B. Martorana and P. Perlo

Fiat Research Center, Orbassano, Italy

1. INTRODUCTION

Currently, there is a very strong interest in using nano-sized metals (i.e., metal clusters containing from 100 to 100,000 atoms) as advanced additives in plastics functionalization, and considerable research activities are being done in this novel field of composite science [1]. Because of surface effects and the dramatic changes in properties occurring when critical lengths governing some physical phenomenon (magnetic, structural, etc.) become comparable with size, nano-sized metals have unique properties (e.g., plasmon absorption, near-IR photoluminescence, superparamagnetism, Coulomb staircase, etc.). The embedding of nanoscopic metal structures into polymeric matrices represents the most simple way to take advantage of some of these novel physical characteristics. Polymer-embedded nanotructures are potentially useful for a

Metal-Polymer Nanocomposites, Edited by Luigi Nicolais and Gianfranco Carotenuto
ISBN 0-471-47131-3

number of technological applications, especially as advanced functional materials (e.g., high-energy radiation shielding materials, microwave absorbers, optical limiters, polarizers, sensors, hydrogen storage systems, etc.) [1]. In addition to the intrinsic nanoscopic material properties and the possibility to make transparent metal–polymer combinations, these materials are interesting also because the presence of a very large filler–matrix interface area can significantly affect the polymer characteristics (e.g., glass transition temperature, crystallinity, free volume content, etc.), allowing the appearance of further technologically exploitable mechanical and physical properties (e.g., fire resistance, low gas diffusivity, etc.).

The control of nanoparticle morphology becomes a very important aspect, since morphology profoundly influences the material performance. As a long-term goal the development of synthesis schemes able to control particle size, shapes, and composition independently from one another is very important, in order to allow tuning of nanocomposite properties.

Metal–polymer nanocomposites can be obtained by two different approaches, namely, *in situ* and *ex situ* techniques. In the *in situ* methods, metal particles are generated inside a polymer matrix by decomposition (e.g., thermolysis, photolysis, radiolysis, etc.) or chemical reduction of a metallic precursor dissolved into the polymer. In the *ex situ* approach, nanoparticles are first produced by soft-chemistry routes and then dispersed into polymeric matrices. Usually, the preparative scheme allows us to obtain metal nanoparticles whose surface has been passivated by a monolayer of *n*-alkanethiol molecules (i.e., C_nH_{2n+1}-*SH*). Surface passivation has a fundamental role since it avoids aggregation and surface oxidation/contamination phenomena. In addition, passivated metal particles are hydrophobic and therefore can be easily mixed with polymers. The *ex-situ* techniques for the synthesis of metal/polymer nanocomposites are frequently preferred to the *in situ* methods because of the high optical quality that can be achieved in the final product.

2. *EX-SITU* SYNTHESIS OF Au-BASED NANOCOMPOSITES

Polymer-embedded gold nanoparticles have been extensively studied [1]. Because of unique physical characteristics, gold–polymer nanocomposites are potentially useful for a number of advanced functional applications, especially in the optical and photonic fields. In particular, these materials can be used as light-stable color filters [2], polarizers [3, 4], ultra-low refractive index materials [5], nonlinear optical devices [6], optical sensors [7], and so on. However, still limited are the chemical routes that allow us to obtain monodispersed thiol-derivatized gold nanoparticles with controlled size to be embedded into poly-

meric matrices. At present, the only method available for the synthesis of thioaurite compounds is that developed by Brust et al. [8]. This technique yields thiol-derivatized gold clusters of moderate polydispersity. However, owing to solubility issues, the method can be applied only to a little number of alkane– or arene–thiol compounds. Such a fundamental restriction prevents the full process exploitation. In addition, the gold particle size can be only lightly modified by adjusting the amount of gold salt. Cluster properties are size-dependent, and the possibility to fine-tune particle dimension is of a fundamental importance in developing functional additives for polymers.

A new method for the controlled synthesis of alkane–thiol-derivatized gold clusters to be used as filler for polymeric nanocomposites has been recently developed by us [9]. This scheme for thiol-derivatized gold clusters preparation involved the mixing under stirring of a poly(*N*-vinyl pyrrolidone) (PVP, Aldrich, M_w = 10,000 amu) solution in ethylene glycol (stabilized at temperatures ranging from 60°C to 110°C) with a little quantity of a concentrated tetrachloroauric acid ($HAuCl_4$, Aldrich) solution in ethylene glycol. For example, in a typical reactive mixture composition, the first solution was prepared by dissolving 4 g of PVP into 20 mL of ethylene glycol, and the second one was prepared by dissolving 5 mg of $HAuCl_4$ in 1 mL of ethylene glycol. After gold nanoparticle formation, the solution had a ruby-red color. In order to end the reaction and to separate nanoparticles, the reactive mixture was cast into a large amount of acetone (250 mL) and the system was sonicated for a few minutes. The Au–PVP nanocomposite system was achieved after flocculation. The product was washed several times with pure acetone and then dried at room temperature under vacuum. The Au–PVP nanocomposite was used as precursor for the thiol-derivatized gold preparation. In particular, the Au–PVP system was dissolved into a dilute ethanol solution of dodecanethiol (DDT, $C_{12}H_{25}$-SH, Aldrich, 98%). DDT acted as a surface passivating agent for gold clusters since it was able to produce a continuous and uniform organic monolayer around them. Thiol molecules bonded the gold surface much stronger than PVP side groups, and therefore the polymeric stabilizer was completely removed from cluster surface, according to a ligand-exchange process:

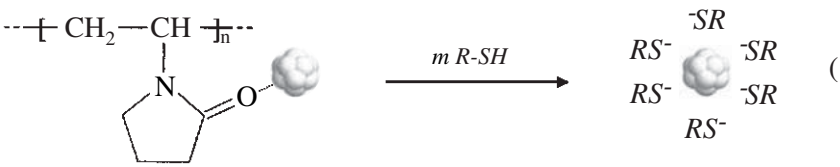

(1)

After two hours the exchange reaction was considered as complete and the hydrophobic thiol-coated nanoparticles were separated from the PVP–ethanol

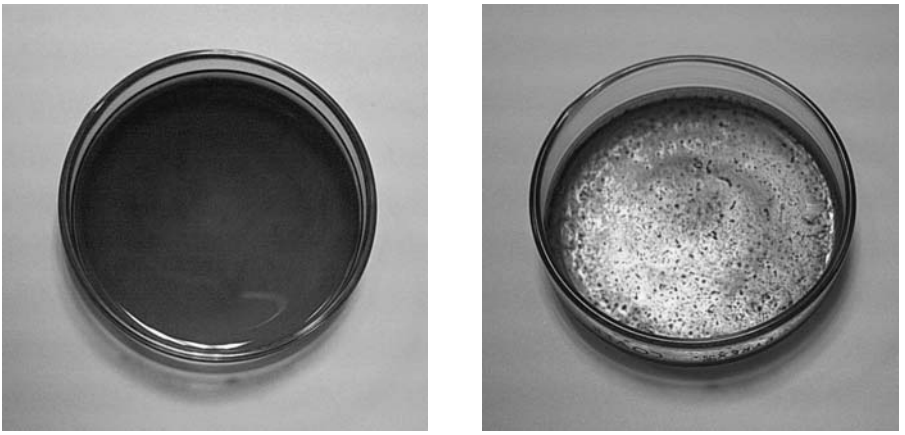

Figure 5.1. Dry thiol-derivatized gold cluster sample.

solution by centrifugation. A waxy, purple solid product with golden shading (see Figure 5.1) was obtained which was accurately washed with ethanol, in order to remove all impurities. This material was stable for months in air at room temperature. Gold–DDT clusters dissolve in hydrocarbons, chlorine solvents, and ethers because of their hydrophobic nature. Clusters were purified by a dissolution/re-precipitation treatment using chloroform and ethanol, respectively.

In order to produce nanocomposite films, thiol-derivatized gold nanoparticles were dispersed in a chloroform solution of polystyrene (PS, Aldrich, M_w = 230,000 amu). High-transparent purple-colored nanocomposite films resulted by solution casting process (see Figure 5.2).

3. Au–PS NANOCOMPOSITE CHARACTERIZATION

The microstructure of both gold clusters embedded into PVP matrices and gold clusters derivatized by dodecanethiol was imaged by transmission electron microscopy (TEM). Transmission electron micrographs were obtained by a Philips EM208S microscope, using an accelerating voltage of 100 kV. Au-clusters–PVP nanocomposites were dissolved in ethanol, and the solution deposited on graphitized Formvar films supported on copper mesh grids for TEM. Heptane was used to disperse alkanethiol-derivatized gold clusters. As visible in Figure 5.3a, all particles had a pseudo-spherical shape which in some cases corresponded exactly to a polyhedron, and aggregates were not present in the samples. The particle size was moderately polydispersed (standard devi-

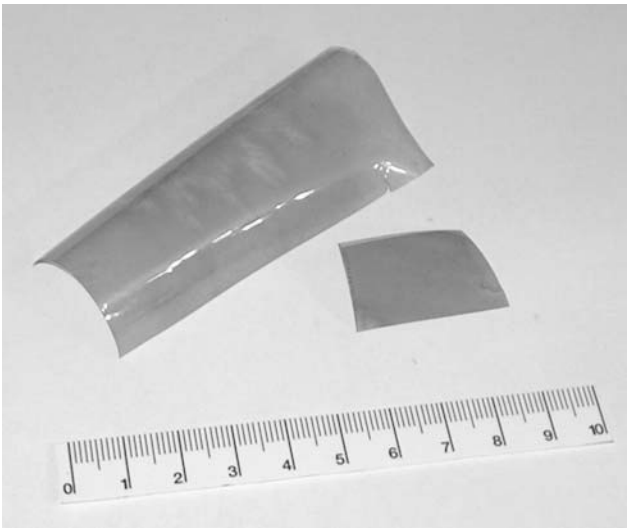

Figure 5.2. Au–PS nanocomposite film.

ation of ~10%) with a monomodal distribution approximately described by a Gaussian function. The particle size distribution was dependent on the reaction conditions (i.e., temperature, time, reactive mixture composition, etc.). However, the most simple way to control the average particle size was by varying the PVP/$HAuCl_4$ weight ratio. In particular, Au clusters with average diameters of 10, 4, and 2 nm were obtained using PVP/$HAuCl_4$ ratios of 400, 800, and 1600 respectively (all reactions were done at 60°C using 21 mL of ethylene glycol and 5 mg of $HAuCl_4$; the reaction time was of 5 min). Therefore, the particle size decreased significantly with increasing of PVP/$HAuCl_4$ weight ratio, allowing us to obtain by the same technique both gold nanoparticles and very small clusters. PVP had a nucleating effect, and therefore higher nucleation rates were obtained by increasing the PVP amount, whereas the cluster growth process was reduced. Sample polydispersity decreased with increasing of PVP amount. Particle size was also dependent on reaction time and temperature; however, such a dependence turned out to be much less sensible and was difficult to control experimentally. Heptane suspensions of gold particles passivated by dodecanethiol spontaneously produced self-organized submicron-sized domains of close-packed nanoparticle arrays by solvent evaporation (see Figure 5.3b). Coalescence aggregates produced by the sintering of the metallic cores were not contained in the final product, thus proving that the ligand-exchange process was really effective and complete.

Figure 5.4 shows the XRD pattern of gold nanoparticles embedded into a PVP matrix. X-ray diffraction measurements were performed with a Rigaku

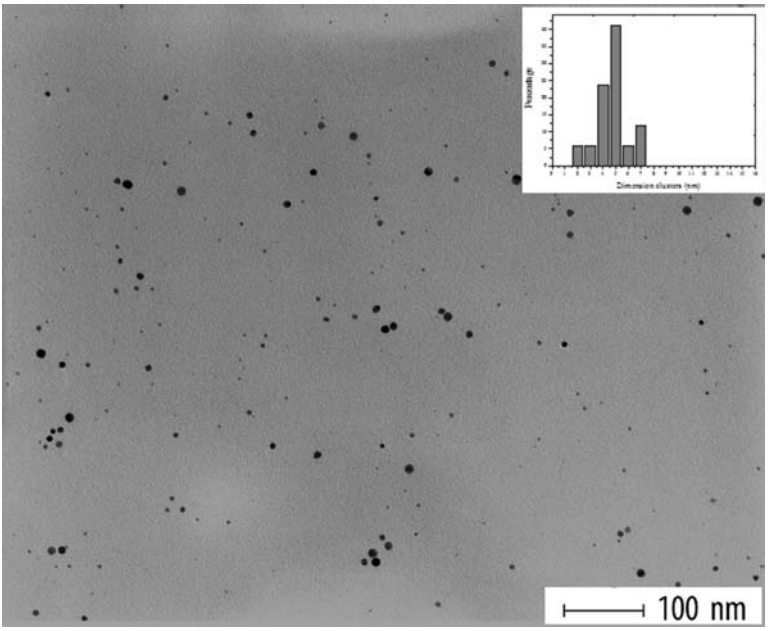

(a)

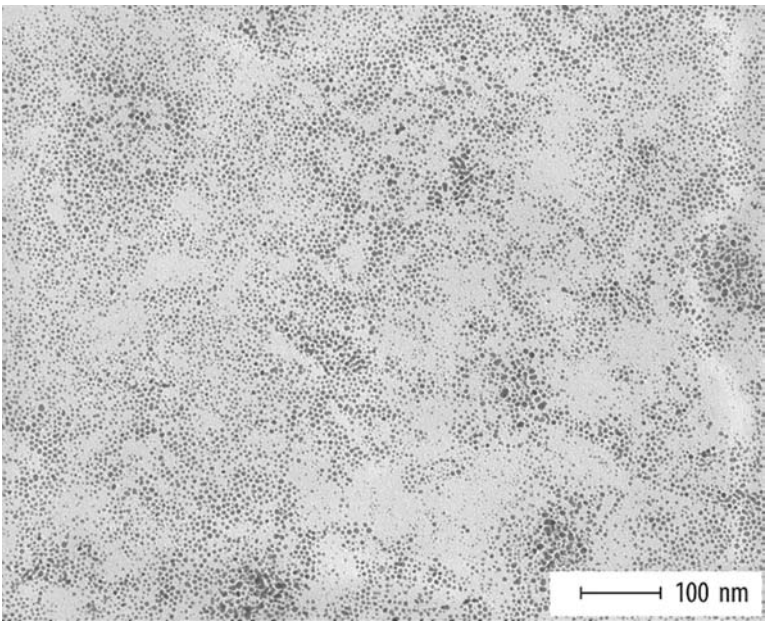

(b)

Figure 5.3. TEM micrographs of **(a)** PVP-embedded gold clusters and **(b)** dodecanethiol-derivatized gold clusters.

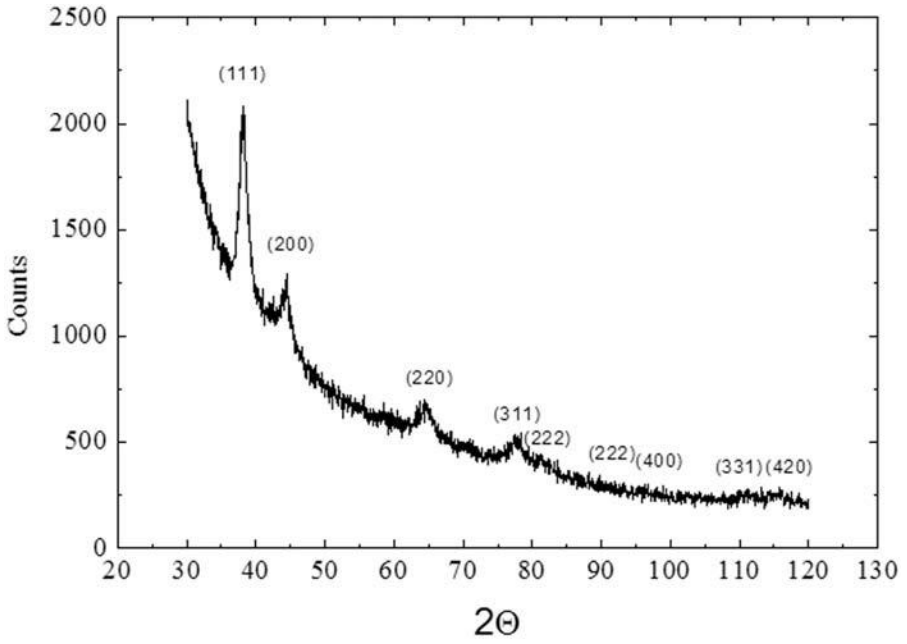

Figure 5.4. XRD pattern of gold nanoparticles embedded into a PVP matrix.

DMAX-IIIC goniometer using Cu-K_α radiation ($\lambda = 0.154056$ nm) and a pyrolytic graphite monochromator in the diffracted beam. The goniometer was operated in the standard Bragg–Brentano $\theta/2\theta$ parafocusing geometry. The spectrum included two broad peaks at $2\theta = 11.5°$ and 21.1° (not visible in Figure 5.4) attributed to the diffraction of the noncrystalline polymer matrix. The spectrum revealed several significantly broad scattering peaks of low intensity; the most evident signals were at 38.2° and 44.6° that can be assigned to the (111) and (200) planes, respectively. The obtained pattern indicated that gold particles were in the face-centered cubic (fcc) structure. The value of the lattice constant calculated from the XRD pattern was $a = 4.0770(7)$ Å, which was consistent with the value for pure bulk gold. The significant broadness of the scattering peaks was caused by the very small size of crystallites. The average size of Au crystals was calculated by Scherrer's equation, and it was determined to be 11.0 ± 0.03 nm for a sample with PVP/$HAuCl_4$ weight ratio of 400. Such value was in good accordance with the corresponding TEM measurement, thus proving a monocrystalline nature of gold clusters.

The formation-growth of gold clusters was monitored by UV–Vis spectroscopy, by looking at the very intensive surface plasmon absorption characterizing nano-sized gold. Optical spectra were recorded at different reaction

times by a UV–Vis spectrophotometer (HP-8453 UV–Vis Spectrophotometer), equipped with a Peltier apparatus to control the reaction temperature with an accuracy of ±0.1°C. The system employed a magnetic stirrer to allow for the homogenization of the reactive mixture and far-UV quartz cuvettes. The temporal size development of clusters was monitored by automatic recording of spectral data on a personal computer connected to the spectrophotometer. The method was very sensitive and allowed for a fast and accurate identification of nanometric solid-phase formation and sizing of resulting spherical particles. The temporal evolution of the UV–Vis spectrum of the reactive mixture is shown in Figure 5.5a. As visible, the spectum is given by the overlap of three different signals: (i) an absorption band at 350 nm produced by the Au^{3+} ions, (ii) a broad absorption band produced by interband transition of gold (from 400 nm to 600 nm), and (iii) the surface plasmon absorption band of gold clusters located at 560 nm. Since the Au^{3+} ions concentration decreases with time being reduced to the zero-valence state, the peak intensity lowered during reaction, assuming negative values. Such a behavior is in accordance with bleaching of yellow color characteristic of gold solutions at the beginning of the reaction. The spectrum convolution by Lorentz's functions (see Figure 5.5b) allows us to accurately measure the features of the plasmon peak (i.e., maximum absorption value and wavelength, full width at half-maximum, integral area, etc.). The analysis of the plasmon peak may give morphological–topological information on the produced cluster system, and in particular the average size of nanoparticles. According to the literature [10], the maximum absorption value, A_{max}, is related to the number of absorption centers, N, and to the average particle radius, R, by the following semiempirical expression:

$$A_{max} = k \cdot N \cdot P^{2.8} \tag{2}$$

where k is a proportionality constant and 2.8 is a semiempirical factor (the theoretical value is 3). Therefore, if the number of gold particles, N, is a constant during the metal phase-separation process, the cubic root of the maximum absorption value is proportional to cluster radius and such information can be used to study the mechanism of cluster growth. The number of metal clusters can be considered as a constant when the nucleation rate is high enough to give separation between nucleation and growth stages [11]. In other words, all cluster nuclei are generated at same time and successively grow together. At temperatures higher than 70°C for a PVP/$HAuCl_4$ weight ratio of 400, the nucleation of gold is fast enough; consequently, nucleation and growth are separated stages of cluster formation, and the number of particles is practically a constant during the radial development of clusters. In this case, a correct evaluation of cluster size can be obtained by using equation (2). However, since the proportionality constant, k, is unknown, TEM calibration, measurements should

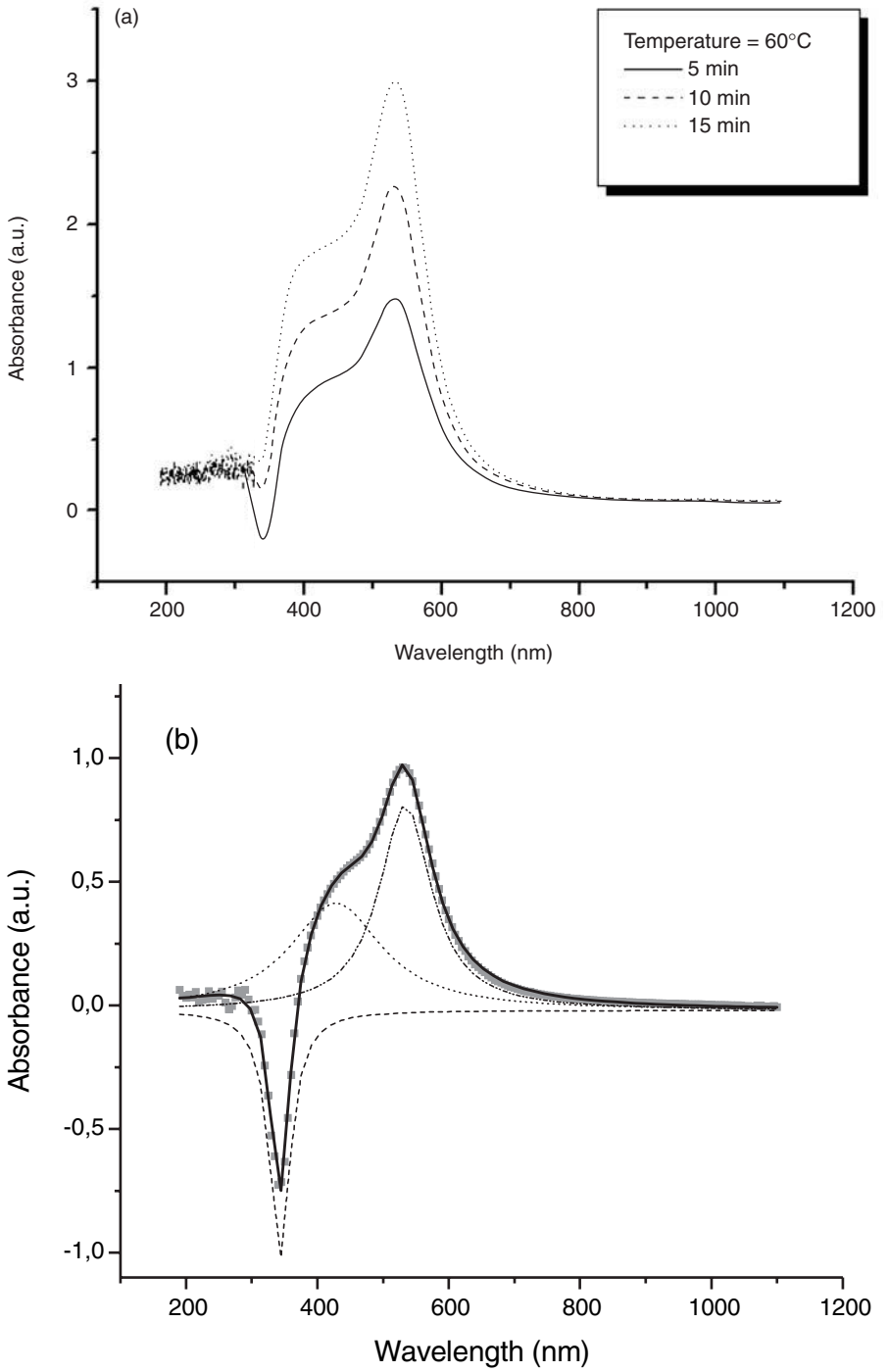

Figure 5.5. Absorption spectra (UV–Vis–NIR) of the reactive $HAuCl_4$–ethyleneglycol–PVP mixture: **(a)** Temporal evolution at 60°C and **(b)** spectrum convolution by Lorentz's functions.

be used. Without calibration, only the profile of the temporal evolution of cluster radius can be obtained. The results of the analysis of spectral data obtained above 70°C by using equation (2) are shown in Figure 5.6a. As visible above 70°C, the cluster radius increased according to a linear function of time. The linear behavior of cluster radius with time is related to the special mechanism of cluster growth that for this system seems to follow a surface-deposition controlled kinetic [12]. Such analysis is in accordance with literature studies for the gold cluster formation by a formaldehyde-based reduction [12]. Figure 5.6b shows the temporal evolution of the maximum plasmon absorbance at temperatures below 70°C. The curve behaved according to a sigmoidal function. The deviation of the cluster radius from the linear behavior and the sigmoidal shape of absorbance versus time plot was probably due to an increase of the cluster number (i.e., the number of absorption centers, *N*) with time as the main phenomena. Consequently, below 70°C, nucleation and growth are not separated stages of the cluster formation process, but they happen simultaneously during the reaction (for a PVP/$HAuCl_4$ weight ratio of 400).

Spectral data showed a partial resolution of interband and plasmon absorption with increasing of reaction temperature. This phenomenon was caused by the thermal expansion of the metal phase which red-shifted the plasmon absorption band.

Samples of pure gold clusters passivated by dodecanethiol were characterized by an endothermic transition well visible in the DSC thermograms. Differential scanning calorimetry (DSC, TA-Instrument Mod.Q100) tests were carried out at 10°C/min under inert atmosphere of dry nitrogen. A sharp endothermic peak appeared at ~30°C, and it was produced by the melting of small crystallites originated from the co-crystallization of interdigitated alkanethiol chains [13]. The melting temperature of interdigitated alkanethiol crystals was much higher than the melting point of pure dodecanethiol (–7°C). When gold clusters derivatized by dodecanethiol molecules were accurately dispersed into a polystyrene matrix, the DSC thermogram of nanocomposite specimens did not show such endothermic transition even for high percentages of gold filler (i.e., up to 30%). The absence of an endothermic transition in the nanocomposite samples indicated the absence of a co-crystallization process among alkanethiol chains of neighbor gold clusters which, according to TEM investigations, proved the contact-free dispersion of passivated gold clusters in polymer.

The thermogravimetric analysis (TGA, TA-Instrument Mod.Q500) of gold clusters derivatized by dodecanethiol showed a weight loss at temperatures above 280°C. The weight loss was produced by the degradation of the organic layer coating the gold cluster surface, which probably occurred according to a dehydrogenation mechanism [14]. The percentage of thiol molecules absorbed on the surface of a monodispersed cluster sample with an average size of

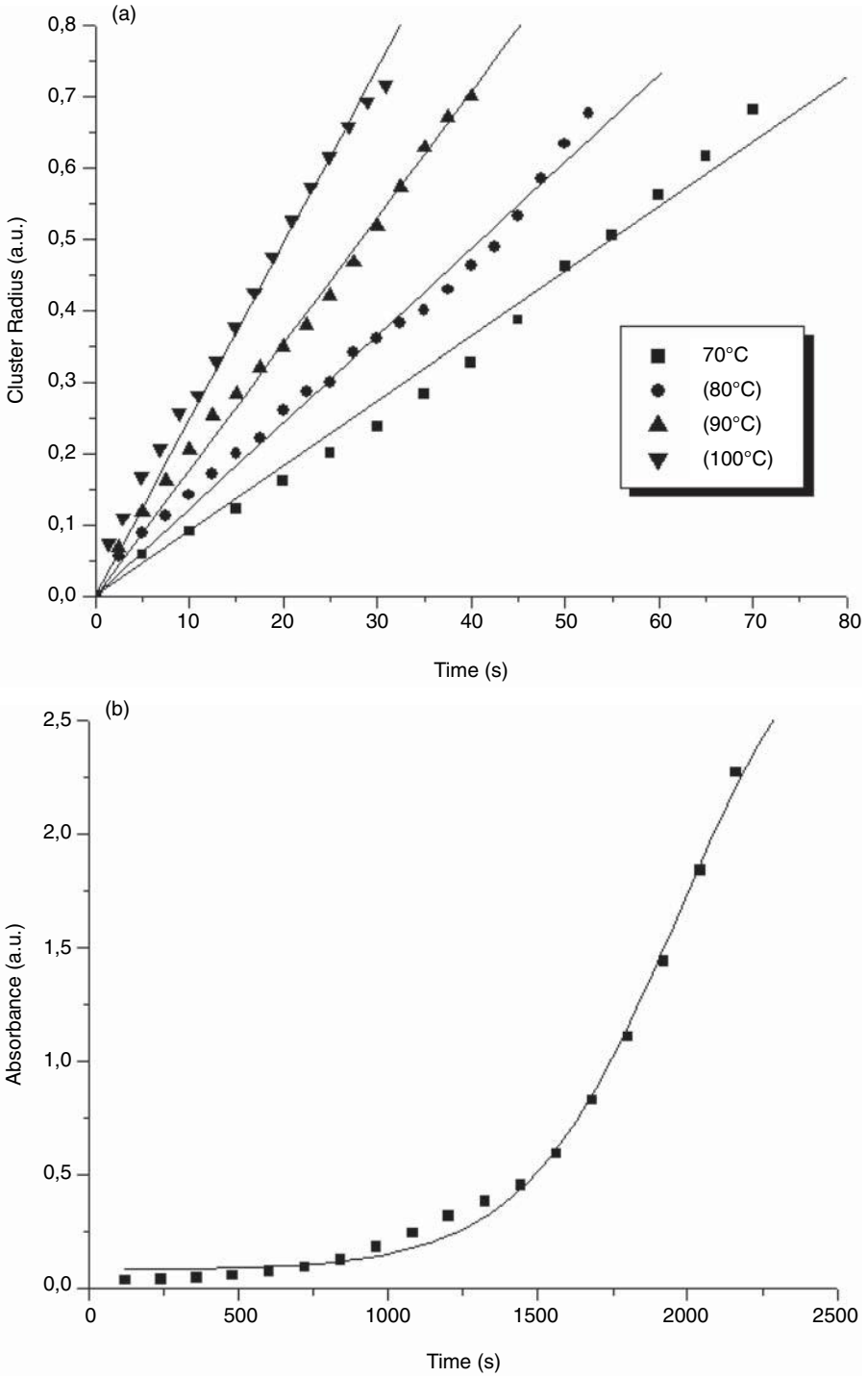

Figure 5.6. Behavior of the cluster radius with time at temperatures above 70°C (**a**), and temporal evolution of absorbance maximum at 25°C (**b**) (in both cases the PVP/$HAuCl_4$ weight ratio was 800).

10 nm was ~80% by weight. Finally, thiol-derivatized gold cluster compounds can be considered as a high-thermally stable substance at dry state.

4. PREPARATION OF NANOCOMPOSITES BASED ON OTHER METALS

Alcoholic reduction and polyol process are well-known and useful chemical routes for the synthesis of nano-sized metal particles [15]. These techniques have been widely used for the preparation of very small clusters of noble metals (e.g., Ag, Au, Pd, Pt, Rh, Ru, Os, Ir, Re, etc.), light transition metals (e.g., Co, Ni, Cu, etc.), and easily reducible metals (e.g., Pb, Sn, Cd, W, Hg). A variety of layered core/shell and alloyed clusters can also be obtained by these approaches [15]. The use of hydrophilic polymers as steric stabilizers (e.g., gelatine, poly(vinylalcohol), poly(acrylic acid), poly(methyl vinyl ether), poly(vinyl pyrrolidone), etc.) are particularly effective, owing to the intensive short-range steric repulsions that these polymers are able to produce. In addition, the use of a polymeric stabilizer is convenient since it allows us to isolate and store clusters in a stable polymer-embedded form, simply by coprecipitation with nonsolvent liquids (e.g., acetone, THF). The resulting composite solid is a hydrophilic material that can be dissolved into a variety of polar liquids. Alcohols are very good solvents for PVP because of the polar nature and low molecular weight (M_w = 10,000 amu). On the other hand, alcohols can dissolve all types of thiol molecules, provided that alcohols with larger hydrocarbon chains are used with increasing of alkane-thiol molecular weight.

Because of the very strong affinity of thiol groups (SH) for the gold surface, the PVP-embedded gold clusters can be used as an excellent precursor material for the thiol-derivatized cluster preparation. Polymer is removed from the gold cluster surface according to a ligand-exchange process. Thiol molecules bond the gold surface by a covalent interaction (i.e., thiol chemisorption) generated from a reduction–oxidation reaction (i.e., $Au_n + m\text{RSH} = Au_n(SR)_m + m/2H_2$), and therefore the physically adsorbed nucleophylic groups of PVP are completely removed from the metal surface. Because of the high solubility of PVP and thiols in polar solvents, a homogeneous-phase reaction is usually involved. Both very small clusters and nanoparticles can be obtained simply by varying the PVP/$HAuCl_4$ weight ratio, and therefore a very general preparative technique that can offer complete control over the metal filler structure results.

Thiol-derivatized gold clusters are materials stable for months in air at room temperature which can be handled like simple chemical compounds. They have a hydrophobic nature and consequently are very soluble in aliphatic and aromatic hydrocarbons (e.g., heptane, cyclohexane, benzene), chlorine solvents (e.g., chloroform, carbon tetrachloride, dichloroethane), and ethers (e.g., diethyl

ether and tetrahydrofuran), only moderately soluble in styrene, and practically insoluble in esters (e.g., methyl methacrylate), acetone, alcohol, and water. Therefore, the product can be easily dispersed into organic solvents able to dissolve hydrophobic polymers like polystyrene. The resulting cluster–polystyrene solutions can be utilized to prepare composite films by solution-casting technology. Because of the small size of gold particles and the amorphous nature of polystyrene, the obtained films do not produce light-scattering phenomena. The elevated transparency of these nanocomposites makes them ideal materials for optical applications.

This novel synthesis scheme has been also investigated with alloyed gold–silver and pure-silver clusters. Ag–Au-alloyed clusters obtained by simultaneous reduction and co-precipitation of two metals give results completely similar to those of the pure-gold clusters. For example, dodecanethiol completely removed PVP from the alloyed cluster surface, producing the thiol derivative. However, the ligand-exchange reaction was not complete in the case of pure-silver clusters embedded in PVP, and consequently the thiolate product isolation–purification was not possible. The success of this chemical technique with other PVP-embedded metal clusters has not be tested yet.

5. *IN SITU* METAL–POLYMER NANOCOMPOSITE SYNTHESIS

A large-scale production of polymer-embedded nano-sized metals should be necessarily based on the thermal decomposition of metal precursors directly added to polymers during their hot–processing stage. A number of organic precursors have been studied for this application [16]; however, any of the tried materials has shown a completely satisfying behavior. We have recently discovered that homoleptic mercaptides (i.e., $Me_x(SR)_y$) can be used as metal precursors in the industrial production of metal–polymer nanocomposites [17]. Mercaptides of transition metals are covalent organic salts characterized by simple synthesis, high compatibility with polymers for the hydrophobic nature, and adequate thermolysis characteristics. These compounds have been occasionally used as polymer additives—for example, for the thermal stabilization of PVC [18]. In particular, mercaptides are quite thermally stable at room temperature, and therefore they can be handled and stored without special care. However, these chemical compounds quantitatively decompose at temperatures that are a little higher (110–180°C), producing zero-valence metal or metal sulfides in addition to organic by-products. The solventless thermolysis of pure mercaptides gives rise mainly to metal sulfides as product [19]. However, mercaptide decomposition in polystyrene matrices frequently produces metal clusters, and the formation of a metal sulfide phase is observed only in presence of high electropositive metals [17]. Such a behavior can be explained on the basis

of a decomposition mechanism of mercaptide in polymeric environments different from that involved in solventless thermolyses.

In this part of the chapter we discuss (a) the controlled thermolysis of thiolate solutions in polystyrene matrix at temperatures above the polymer glass transition temperature and (b) the reaction mechanism in the case of silver–polystyrene nanocomposite systems. However, the same reaction mechanism is probably involved in the thermolysis of other mercaptide–polystyrene systems. This technique has proven to be an excellent new preparative scheme for the generation of both metal and sulfide clusters in polymers. In particular, high-molecular-weight *n*-alkanethiolates have shown to be the most effective compound class since the low volatility of thermolysis by-products avoids film foaming during the annealing process.

6. METAL PRECURSOR SYNTHESIS

Usually, high-molecular-weight *n*-alkanethiolates are not commercially available products, but their synthesis is very simple, and only common chemical reagents are required. In particular, thiolates of different metals (e.g., Co, Pd, Pb, Cd, Cu, Au, Ag, etc.) were obtained according to the following general preparative scheme. Metal salts quite soluble in alcohols (e.g., acetates) were selected for this reaction. A few milliliters of alkanethiol (e.g., C_{12}, C_{16}, or C_{18} thiols, Aldrich 98%) were dissolved in ethanol and added dropwise (under stirring, in ~15 min) to a stoichiometric quantity of a metal salt solution in ethanol. The reaction was performed at room temperature, and reagents were used without purification. During thiol solution addition, the system becomes a slurry because of thiolate precipitation. Reaction yields close to 100% resulted, owing to the very low thiolate solubility in the alcoholic medium. In particular, for the reductive nature of thiols, changes in the metal oxidation number were also possible before precipitation. When there were no changes in the metal oxidation number (e.g., with Cu^{2+}, Pb^{2+}, and Pd^{2+} ions), the precipitation promptly occurred; whereas precipitation required some time to take place in the case of an oxidation number variation (e.g., Au(I)–S–R formation from Au(III) salts). Depending on the metal nature and therefore on the ability for the metal thiolate to produce polymeric structures, the product texture was ranging from waxy or rubbery (polymeric thiolates) to a powdered crystalline material. The metal thiolates were separated by vacuum filtration and washed several time by acetone, and then they were purified by dissolution in hot chloroform (50°C) and re-precipitated by ethanol addition.

Owing to the slow dissolution kinetic and limited solubility of silver salts in alcohols, silver dodecyl mercaptide, $AgSC_{12}H_{25}$, has been prepared by adding drop-by-drop an acetone solution of dodecanethiol ($C_{12}H_{25}SH$, Aldrich) to a

silver nitrate solution ($AgNO_3$, Aldrich, 99.9%) in acetonitrile at room temperature, under stirring [20]. Stoichiometric amounts of unpurified reactants were used. A white crystalline powder promptly precipitated. The Ag–mercaptide powder was separated by pump filtration and washed several times with acetone. The XRD pattern of silver dodecyl mercaptide showed a periodicity at low Bragg's angles, characteristic of a lamellar structure. According to the literature, such texture causes scarce solubility of this chemical compound in organic solvents [21]. The dry powder was stable for months at room temperature, but Ag-thiolate solution–dispersion in organic solvents showed a scarce stability and became brown in a few days.

7. NANOCOMPOSITE PREPARATION

Nanocomposite preparation will be illustrated considering the Ag–polystyrene systems. To prepare silver–polystyrene nanocomposite films, $AgSC_{12}H_{25}$ was dissolved/dispersed in chloroform, and this solution mixed with a chloroform solution of polystyrene (Aldrich, $M_w = 230{,}000$ amu). The obtained white slurry was cast onto a glass substrate (Petri dishes) and allowed to dry at room temperature. Dry $AgSC_{12}H_{25}$–polystyrene blends were homogeneous and transparent. This material was removed from the glass surface and annealed at ~150°C using a hot plate. During the thermal treatment, the transparent precursor films soften and slowly became light yellow. Little amounts of gas evolved from the viscous polymer phase during annealing with small bubble formation. The color of annealed film promptly changed from yellow to dark brown by cooling the material at room temperature. A prompt chromatic variation always was observed by heating the samples at temperatures higher than the polymer glass transition temperature (T_g), and the color transition was completely reversible. The intensity of this thermochromic effect depended on the quantity of the silver phase contained inside the polymer films (i.e., films changed from black to light brown at high silver contents, and from dark brown to light yellow at low silver content). However, this phenomenon was observed also in the presence of very small silver amounts. Excessively long annealing treatments of precursor film caused the formation of a silver mirror inside the polymeric material, probably because of sintering processes.

The nanocomposite films were purified by prolonged dipping in acetone. In particular, polystyrene became swollen by acetone absorption, and all organic by-product completely diffused outside. In addition, thermochromic layers of very uniform thickness were obtained by dissolving the nanocomposite material in adequate quantities of chloroform and spin-coating the obtained viscous solutions on polymeric substrates (e.g., PET films).

8. NANOCOMPOSITE FILM CHARACTERIZATION

The microstructure of obtained nanocomposite materials was imaged by transmission electron microscopy (TEM). In the preparation of TEM specimens, the nanocomposite material was dissolved in heptane, and drops of the solution were placed on a Formovar-covered copper grid. The dry films were then sputtered by graphite. Transmission electron micrographs were obtained by a Philips EM208S microscope, using an accelerating voltage of 100 kV. Figure 5.7a shows the inner structure of a nanocomposite sample obtained by annealing a $Pd(SC_{12}H_{25})_2$–PS blend for 5 min at 170°C. As visible, a uniform, contact-free distribution of metal particles resulted inside this film. Particles were sufficiently monodispersed with an average size of 10 nm and did not produce aggregates; in addition, they showed a spherical shape. However, as shown in Figure 5.7b, a special inner morphology characterized films of gold clusters embedded in polystyrene. In these nanocomposite films, the clusters were organized in two-dimensional superstructures of different extensions. Such a special topology of nanocomposite films was not observed with other types of metal particles. Figure 5.7c shows the special topology originated inside the

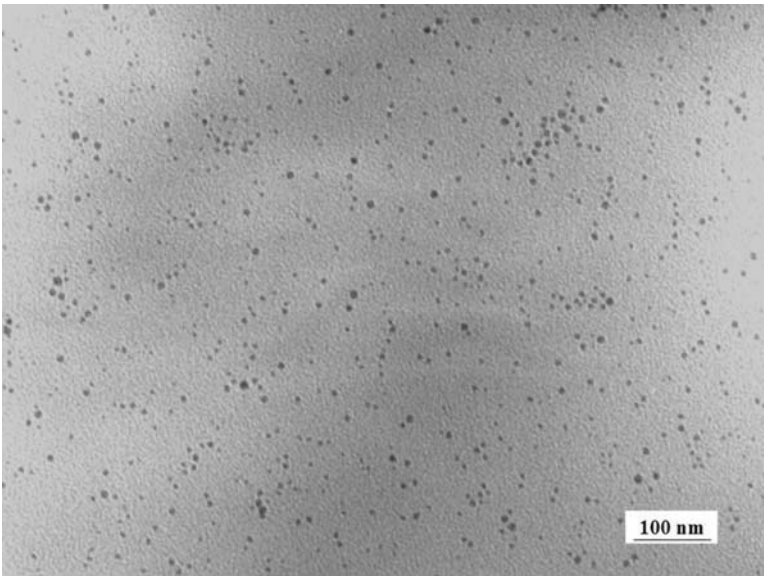

(a)

Figure 5.7. TEM micrographs of polystyrene-embedded metal clusters: (**a**) Palladium ($Pd(SC_{12}H_{25})_2$–polystyrene was annealed at 170°C for 5 min), (**b**) gold ($AuSC_{12}H_{25}$–polystyrene was annealed at 180°C for 5 min), and (**c**) silver ($AgSC_{12}H_{25}$–polystyrene was annealed at 150°C for 1 min).

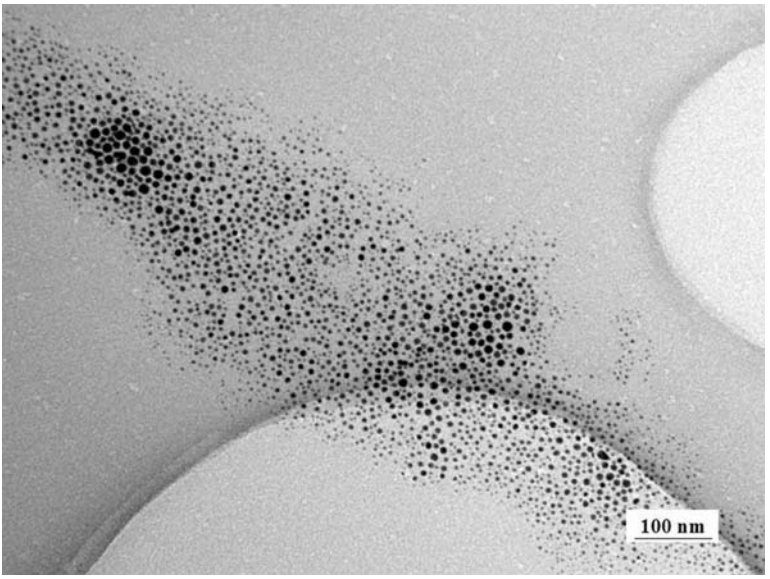

(b)

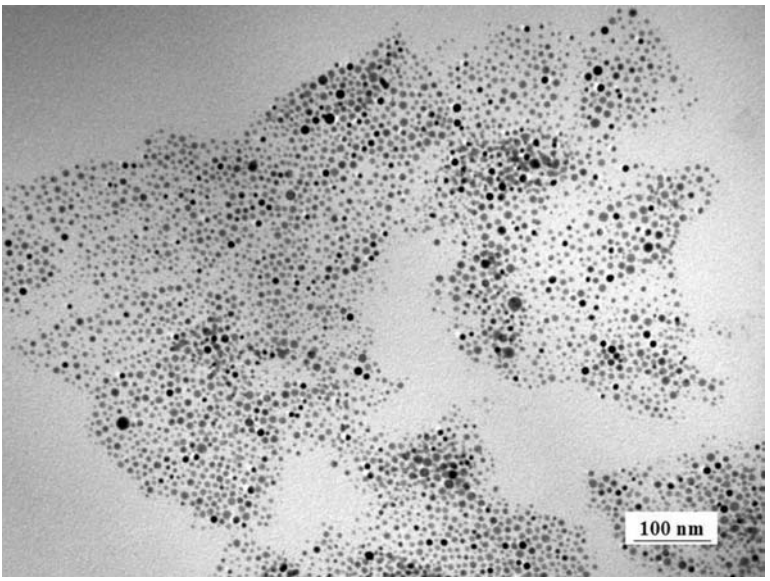

(c)

Figure 5.7. Continued

$AgSC_{12}H_{25}$–polystyrene films during thermal treatment. As visible, large two-dimensional domains of aggregated silver nanoparticles were originated by mercaptide decomposition in molten polymer. Silver aggregates had different shapes and size, and the included silver nanoparticles were not sintered together but were contact-free and uniformly distributed. Such a special microstructure was probably caused by the presence of a polystyrene phase among neighbor silver particles. In a typical preparation (i.e., 11.5% by weight of dodecyl mercaptide, annealed at 150°C for 5 min) the resulting silver clusters were polydispersed and had an average size of 8.0 nm, with a monomodal Gaussian size distribution.

Some mercaptide–polystyrene blends (e.g., $Pb(SC_{12}H_{25})_2$–PS, $AgSC_{12}H_{25}$–PS) were not stable at room temperature over a long time period. Figure 5.8a shows the inner structure of a $AgSC_{12}H_{25}$–polystyrene film aged for 8 weeks at 25°C. The silver clusters had a very small size (~1.8 nm) and were monodispersed and uniformly dispersed in the embedding polymeric matrix. Figure 5.8b shows the inner structure of a $Pb(SC_{12}H_{25})_2$–polystyrene aged for 12 weeks at 25°C.

When metals characterized by a surface plasmon absorption (e.g., gold and silver) were generated by this technique inside the polystyrene matrix, the nanocomposite films developed the characteristic color of the nano-sized metal. In particular, polystyrene films containing silver dodecyl thiolate developed a yellow color during the annealing treatment which changed to brown by cooling down the films, and polystyrene films containing gold thiolate developed a blue coloration. The presence of metal nanoparticles with plasmon absorption inside the polystyrene matrix can be sensibly detected by UV–Vis spectroscopy, because of the strong molar extinction characterizing these nano-sized metals. In particular, Figure 5.9a shows the optical spectrum of a silver–polystyrene nanocomposite sample dissolved in chloroform. As visible, in addition to the characteristic absorptions of polystyrene (from 200 nm to 260 nm), the spectrum also contains a broad absorption band located at ~430 nm corresponding to the silver surface plasmon absorption. Analogously, the presence of zero-valence gold nanoparticles inside the polystyrene matrix can be sensibly detected by UV–Vis spectroscopy, because of the characteristic surface plasmon absorption band of gold particles (see Figure 5.9b).

Figure 5.10 shows optical spectra of an Ag–PS nanocomposite film at two different temperatures (25°C and 110°C). These spectra were obtained by heating a nanocomposite film in the sampling chamber of the UV–Vis–NIR spectrophotometer. The spectrum at higher temperatures results from electronic absorptions of matrix and surface plasmon resonance of embedded silver nanoparticles (i.e., isolated Ag particles, absorbing at ~430 nm). At room temperature, a broad absorption band extending to most of visible spectral region was observed. This thermochromic effect characterizing the nanocomposite

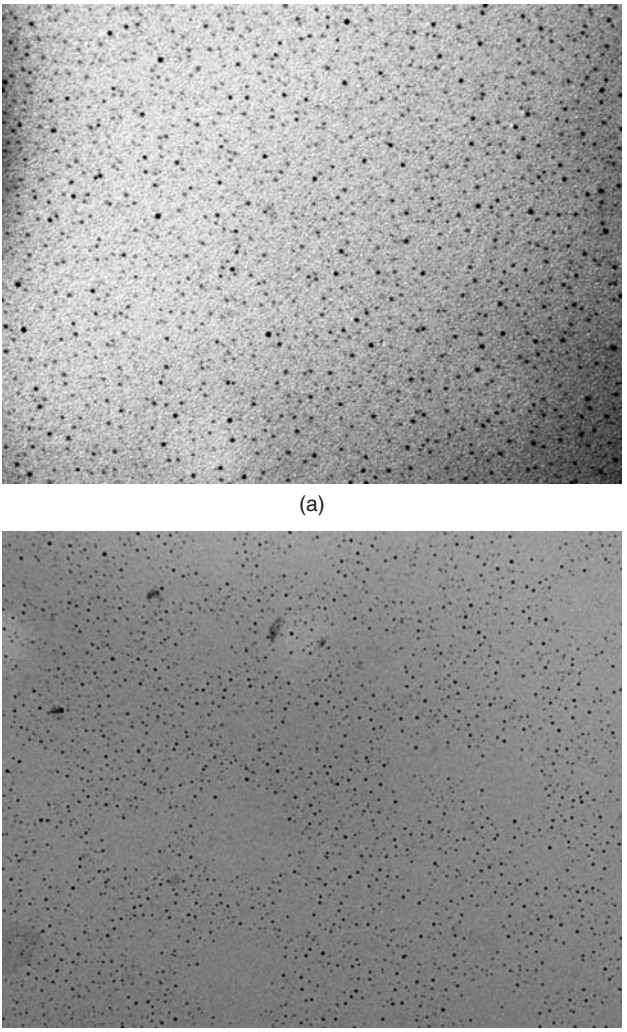

(a)

(b)

Figure 5.8. Mercaptide–polystyrene blends aged for a long time: (**a**) $AgSC_{12}H_{25}$–polystyrene aged for 8 weeks at 25°C, and (**b**) $Pb(SC_{12}H_{25})_2$–polystyrene aged for 12 weeks at 25°C.

films was probably related to the special nanocomposite microstructure, made of large nanoparticle aggregates. In fact, silver clusters are characterized by optical absorption in the visible region because of surface plasmon resonance. However, owing to dipole–dipole interactions, aggregated particles have optical absorption different from that of isolated particles. In particular, at short interparticle distances, the interactions among particle dipoles cause a multiple

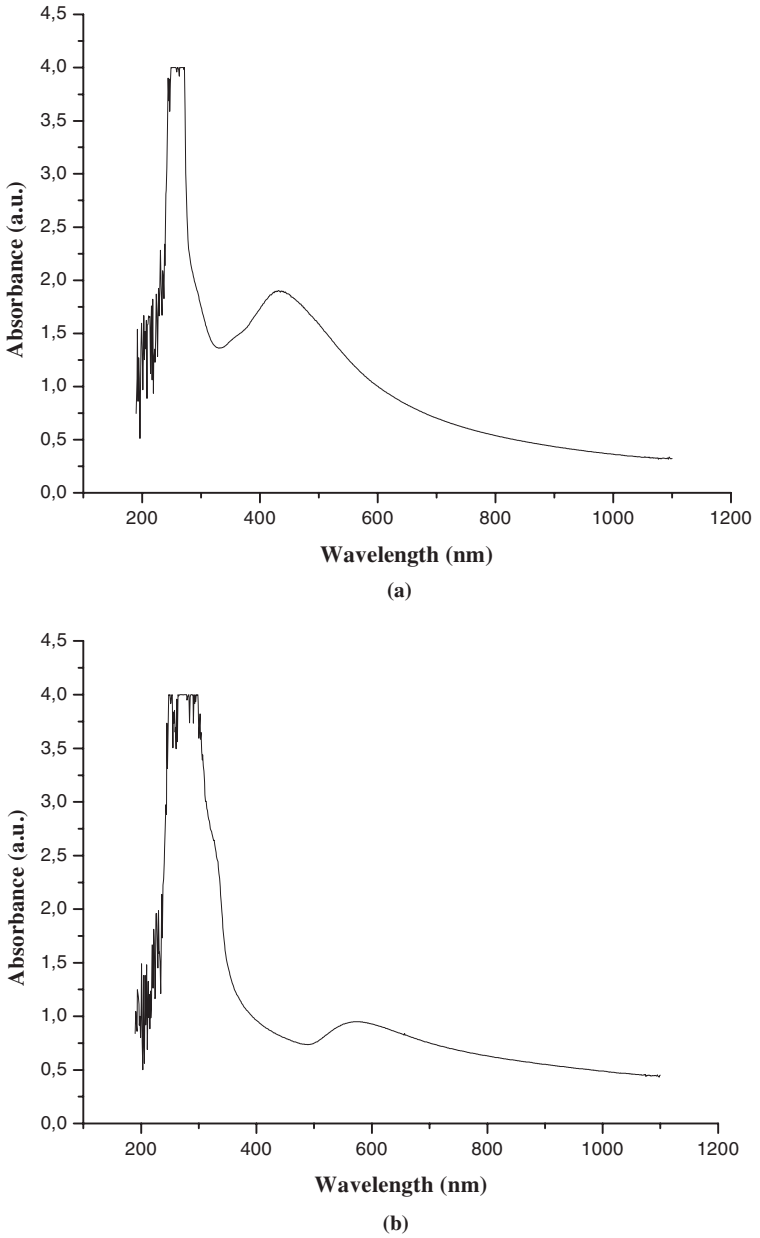

Figure 5.9. UV–Vis spectra of nanocomposite samples dissolved in chloroform: (**a**) Ag–PS and (**b**) Au–PS.

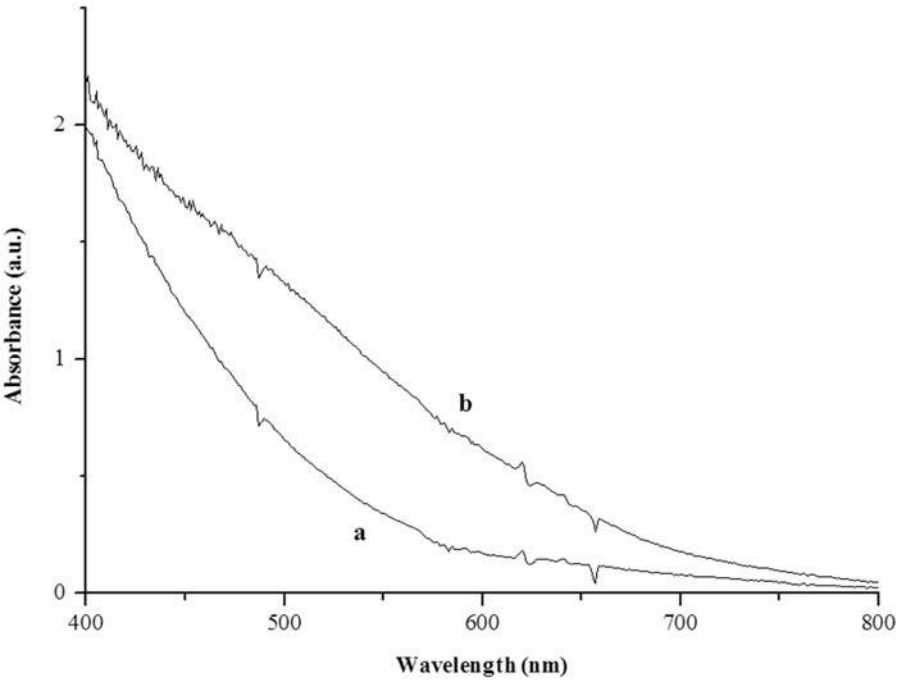

Figure 5.10. UV–Vis spectrum of Ag–PS at (**a**) 25°C and (**b**) 110°C.

splitting of silver surface plasmon absorption and consequently a broad optical absorption. Nanocomposite heating above the polystyrene glass transition temperature causes expansion of aggregates with significant increase in the interparticle distance and transition from "collective" surface plasmon absorptions to "individual" particle optical absorptions [22]. Such chromatic variation of polystyrene films filled by silver clusters can have important technological application, for example, in the area of thermal and chemical sensors. Gold-filled polystyrene films appeared dichroic; in particular, they appeared red or blue depending on the observation direction. Such a phenomenon was probably generated by the particular acicular shape of gold aggregates present in the films [1].

9. THERMOLYSIS MECHANISM

The mechanism involved in the marcaptide termolysis was investigated in the case of silver-based nanocomposite formation. Silver nanoparticles were completely removed from the polymeric matrix by prolonged centrifugation (30 min) of nanocomposite samples dissolved in chloroform at 13,000 rpm, and

the isolated polystyrene was characterized by UV–Vis spectroscopy both as solid and chloroform solution. In addition to the characteristic absorptions of polystyrene phenyl side groups (i.e., $\pi \rightarrow \pi^*$ transitions at 200, 230, and 260 nm), the UV–Vis spectrum of solid film (see Figure 5.11a) revealed the presence of a broad absorption band whose maximum is located at ~350 nm. As visible in Figure 5.11b, when the optical spectrum was obtained from solution, the resulting peak split in two components located at 330 nm and 360 nm. Such absorptions indicated the presence of conjugated biphenylbutadiene groups along the polymer chains (in particular, sterically hindered *trans*-diphenylbutadiene groups should be present in the polymer chain [23]). Therefore, the polymer should participate in the thermolysis process and undergo a hydrogen abstraction reaction with formation of carbon–carbon double bonds in the chains. The UV–Vis characterization of silver particles isolated by centrifugation revealed the presence of polystyrene, which probably formed a network around silver particles in the aggregates (see Figure 11c). Heating in boiling solvent (decane) and/or prolonged sonication of separated silver nanoparticles did not allow the polystyrene removal from particles. Consequently, in addition to hydrogen abstraction, also polystyrene crosslinking processes should happen during the thermolysis reaction.

The cleavage of S–C bond in the silver mercaptide compound was calorimetrically studied. In particular, $AgSC_{12}H_{25}$–polystyrene blends were subjected to annealing treatments in a differential scanning calorimeter (DSC, TA Instruments, DSC-2920) at 10°C/min under the inert atmosphere of dry nitrogen. A typical DSC thermogram of nanocomposite samples is shown in Figure 5.12. As visible, the DSC thermogram included an endothermic peak at ~60°C, produced by the melting of silver thiolate phase, and a stronger endothermic peak at ~110°C, which according to the literature [19] was produced by the cleavage of S–C bond in the thiolate molecules. Above that temperature, the baseline of DSC termogram became very noisy. Such a phenomenon was probably due to the formation of volatile by-products, which gradually diffused through the film and evaporated at film surface, giving a number of very small endothermic peaks. The DSC thermogram included also an inflection in the baseline at 95°C; this signal was produced by the polystyrene glass-transition temperature.

According to UV–Vis and DSC observations, the mechanism for zero-valence silver formation inside polystyrene matrices should involve a reduction of silver ions by hydrogen atoms generated from polystyrene during thermolysis. In particular, according to the DSC thermogram, the Ag-mercaptide

Figure 5.11. UV–Vis spectra of (**a**) solid nanocomposite matrix (**insert**: pure polystyrene), (**b**) nanocomposite matrix in chloroform (**insert**: 1,4-dipheny-l,3-butadiene), and (**c**) nanocomposite filler (silver nanoparticles).

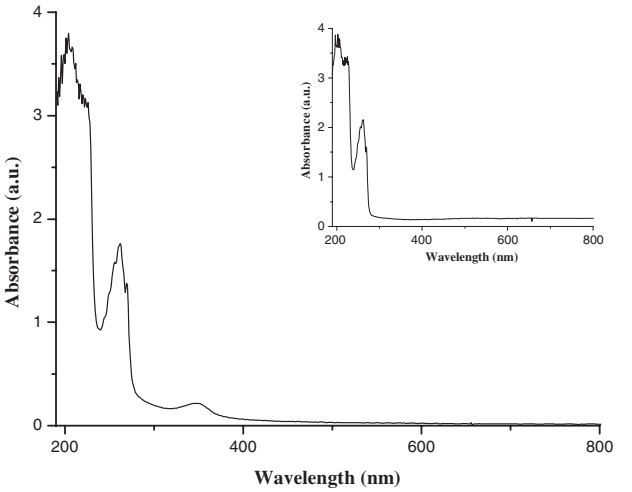

(a)

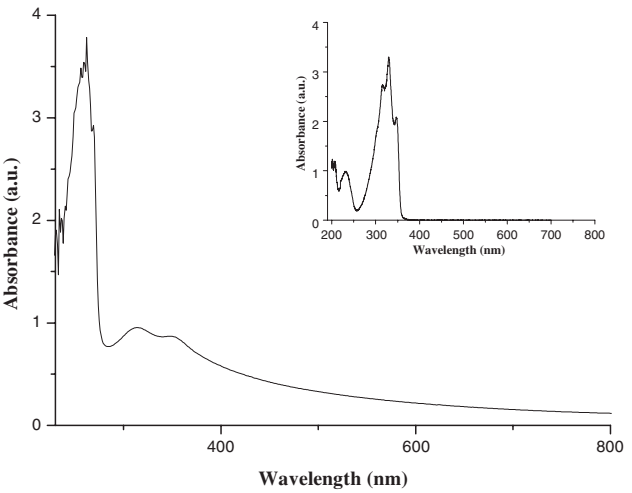

(b)

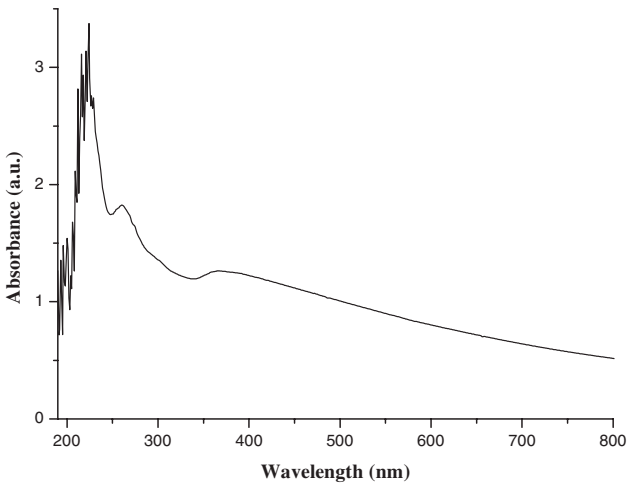

(c)

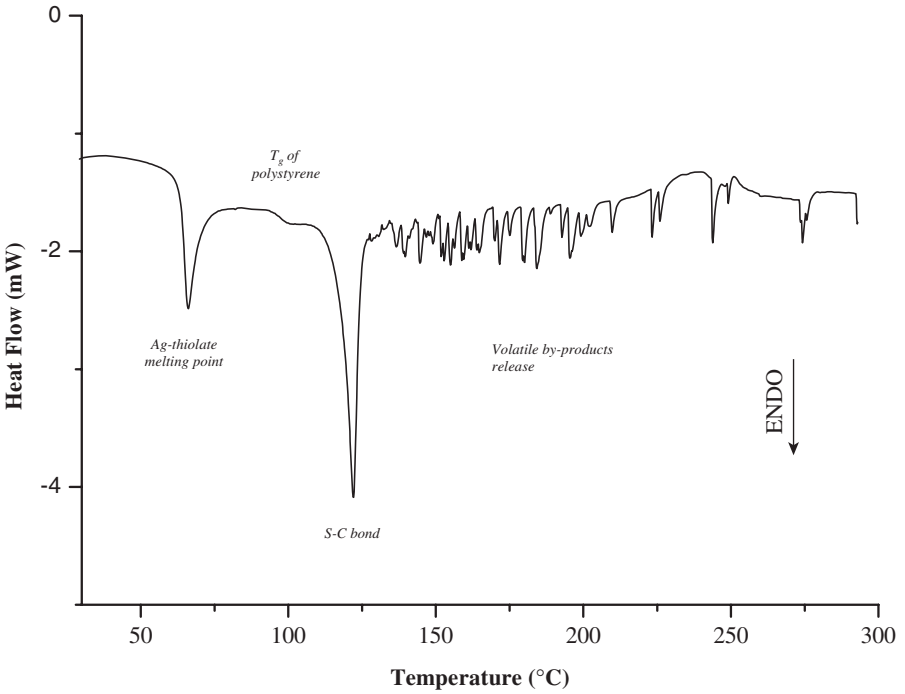

Figure 5.12. DSC thermogram of a $AgSC_{12}H_{25}$–polystyrene blend (10°C/min, under fluxing nitrogen).

molecules dissolved in the molten polystyrene matrix spontaneously decompose and generate alkyl, R·, and metal sulfide, AgS·, radicals by heating at 110°C through an S–C bond cleavage reaction:

$$\text{Ag–S–R} \rightarrow \text{Ag–S}\cdot + \text{R}\cdot \tag{3}$$

Since these molecular fragments are produced in a hydrogen-rich environment, they promptly stabilize by hydrogen abstraction from the surrounding hydrocarbon polymer. This process produces dodecane and acid metal sulfide species, in addition to polystyryl radicals. Hydrogen atoms should be principally removed from tertiary carbons in the polymer chains, because in this case resonant-stabilized carbon radicals result:

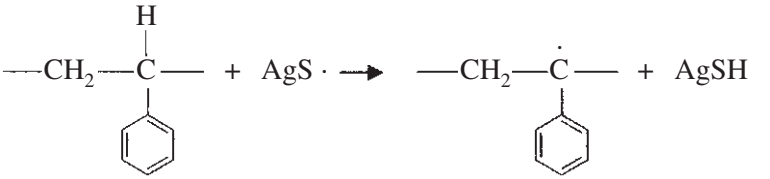

(4)

As known from studies on the mechanism of styrene radical polymerization, the generated carbon radicals may stabilize by β-elimination of hydrogen, producing conjugated double bonds in the polymer chain or bond together, creating a crosslinked three-dimensional network.

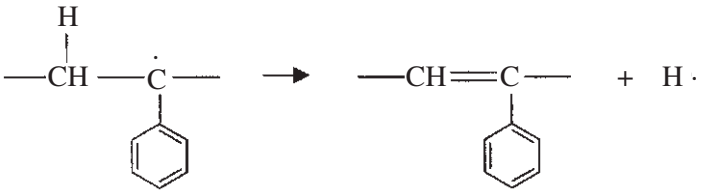

(5)

The free hydrogen atoms generated in the system may reduce silver ions to zero-valence state, giving H_2S as a by-product. Atomic hydrogen may also combine to produce molecular hydrogen and/or reduce directly silver mercaptide molecules to give silver atoms and alkyl–thiol that absorbs on the cluster surface. The presence of diphenylbutadiene groups in the polymer chain can be explained on the basis of the extremely easy abstraction of hydrogen atoms near the styryl groups.

According to this reaction mechanism, zero-valence metals are obtained with all those metal ions easily reducible by hydrogen (e.g., Au, Ag, Pd, Pt, Cu, etc.), whereas metal sulfides result when the thermal decomposition (calcinations) of the acid metal sulfide produced during thermolysis is the only possible chemical process (e.g., Cd, Zn, etc.):

$$Cd(SH)_2 \rightarrow CdS + H_2S\uparrow \tag{6}$$

10. CONCLUSION

In this chapter, two new approaches for the synthesis of metal–polymer nanocomposite materials have been described. The first method allows the preparation of contact-free dispersions of passivated gold clusters in polystyrene, and it is based on a traditional technique for the colloidal gold synthesis—that is, the alcoholic reduction of tetrachloroauric acid in presence of poly(vinyl pyrrolidone) as polymeric stabilizer. The primary function of the stabilizer is to avoid cluster sintering, but it also allows us to isolate clusters by co-precipitation. It has been found that the obtained polymer-protected nanometric gold particles can be dissolved in alkane–thiol alcoholic solutions to yield thiol-derivatized gold clusters by thiol absorbtion on the metal surface. Differently from other approaches for thioaurite synthesis available in the literature, this method allows complete control over the passivated gold cluster structure since a number of thiol molecules can be equivalently used and the

metal core size can be accurately varied by modifying the reactive mixture composition. The same technique can be utilized also for the preparation of cluster compounds of other metals. The second preparative approach describes the use of homoleptic mercaptides as an effective additive for plastic metallation. This method makes it possible to generate dispersions of monodisperse nanoparticles in the polymeric matrix with sizes and filling factors that can be tuned simply by varying the amount of dissolved thiolate precursor and annealing time or temperature. Alkanethiolates of transition metals are organic compounds characterized by a combination of chemical and physical properties really adequate for the generation of nano-sized metal or sulfide inclusions in polymers. In particular, these compounds can be easily synthesized and have a hydrophobic nature compatible with most polymers. In addition, the mercaptide thermolysis occurs at moderately low temperatures (150–200°C), but these compounds are sufficiently stable at room temperature, and consequently they can be handled and stored without special care.

REFERENCES

1. G. Carotenuto and L. Nicolais, Nanocomposites, Metal-Filled, in the *Encyclopedia of Polymer Science and Technology*, Wiley, New York (2003); W. Caseri, *Macromol. Rapid Commun.* **21**, 705–722 (2000).
2. A. G. deLeon, Y. Dirix, Y. Staedler, K. Feldman, G. Hahner, W. R. Caseri, and P. Smith, *Appl. Opt.* **39**(26), 4847–4851 (2001).
3. A. H. Lu, G. H. Lu, A. M. Kessinger, and C. A. Foss, *J. Phys. Chem B* **101**(45), 9139–9142 (1997).
4. Y. Dirix, C. Darribere, W. Heffels, C. Bastiansen, W. Caseri, and P. Smith, *Appl. Opt.* **38**(31), 6581–6586 (1999).
5. L. Zimmerman, M. Weibel. W. Caseri, U. W. Suter, and P. Walther, *Polym. Adv. Technol.* **4**, 1–7 (1993).
6. G. L. Fisher and R. W. Boyd, in *Nanostructured Materials Cluster, Composites, and Thin Films*, edited by V. M. Shalaev and M. Moskovits, Washington, DC (1998), p. 108.
7. R. D. Harris and J. S. Wilkinson, *Sensors and Actuators B* **29**, 261–267 (1995).
8. M. Brust, M. Walker, D. Bethell, D. J. Schiffrin, and R. Whyman, *J. Chem. Soc., Chem. Commun.* **15**, 801–802 (1994).
9. G. Carotenuto and L. Nicolais, *J. Mater. Chem.* **13**, 1038–1041 (2003).
10. J. Turkevich, P. C. Stevenson, and J. Hillier, *Discuss. Faraday Soc.* **11**, 55–75 (1951).
11. T. Sugimoto, *Adv. Colloid Interface Sci.* **28**, 65–108 (1987).
12. R. Zsigmondy and E. Hückel, *Z. Phys. Chem.* **116**, 291–305 (1925).

13. R. H. Terril, T. A. Postlethwaite, C. H. Chen, C. D. Poon, A. Terzis, A. Chen, J. E. Hutchinson, M. R. Clark, G. Wignall, J. D. Londono, R. Superfine, M. Falvo, C. S. Johnson, Jr., E. T. Samulski, and R. W. Murray, *J. Am. Chem. Soc.* **117**, 12537–12548 (1995); T. Prozorov and A. Gedanken, *Adv. Mater.* **10**(7), 532–535 (1998).
14. C. M. Friend and D. A. Chen, *Polyhedron* **16**(18), 3165–3175 (1997).
15. F. Fievet, in *Fine Particles Synthesis, Characterization, and Mechanism of Growth*, edited by T. Sugimoto, New York (2000), pp. 460–496.
16. A. B. R. Mayer, *Mater. Sci. Eng. C* **6**, 155–166 (1998).
17. G. Carotenuto, B. Martorana, P. Perlo, and L. Nicolais, *J. Mater. Chem.* **13**, 2927 (2003).
18. L. Qu, W. Tian, and W. Shu, *Polym. Degrad. Stab.* **76**, 185–189 (2002).
19. M. B. Sigman, A. Ghezelbash, T. Hanrath, A. E. Saunders, F. Lee, and B. A. Korgel, *J. Am. Chem. Soc.* **125**, 16050–16057 (2003).
20. I. G. Dance, K. J. Fisher, R. M. Herath Banda, and M. L. Scudder, *Inorg. Chem.* **30**, 183–187 (1991).
21. P. J. Thomas, A. Lavanda, V. Sabareesh, and G. U. Kulkarni, *Proc. Indian Acad. Sci. (Chem. Sci.)* **113**, 661–619 (2001).
22. U. Kreibig, M. Quinten, and D. Schoenauer, *Phys. Scripta* **T13**, 84–92 (1986).
23. R. L. Rucker, B. J. Schwartz, M. A. El-Bayoumi, and C. B. Harris, *Chem. Phys. Lett.* **235**, 471–478 (1995).